Xinyu Liu
Keekyoung Kim
Yong Zhang
Yu Sun

Advanced Micro and Nanosystems Laboratory,
University of Toronto, Ontario,
Canada
sun@mie.utoronto.ca

Nanonewton Force Sensing and Control in Microrobotic Cell Manipulation

Abstract

Cellular force sensing and control techniques are capable of enhancing the dexterity and reliability of microrobotic cell manipulation systems. In this paper we present two experimental techniques for nanonewton force sensing and control in microrobotic cell manipulation. A vision-based cellular force sensing approach, including a microfabricated elastic cell holding device and a sub-pixel visual tracking algorithm, was developed for resolving forces down to 3.7 nN during microrobotic mouse embryo injection. The technique also experimentally demonstrated that the measured mechanical difference could be useful for in situ *differentiation of healthy mouse embryos from those with compromised developmental competence without requiring a separate mechanical characterization process. Centered upon force-controlled microrobotic cell manipulation, this paper also presents nanonewton force-controlled micrograsping of interstitial cells using a microelectromechanical systems (MEMS)-based microgripper with integrated two-axis force feedback. On-chip force sensors are used for detecting contact between the microgripper and cells to be manipulated (resolution: 38.5 nN at 15Hz) and sensing gripping forces (resolution: 19.9 nN at 15Hz) during force-controlled grasping. The experimental results demonstrate that the microgripper and the control system are capable of rapid contact detection and reliable force-controlled micrograsping to accommodate variations in size and stiffness of cells with a high degree of reproducibility.*

KEY WORDS—microrobotic cell manipulation, cellular force measurement, nanonewton force sensing and control, sub-pixel visual tracking, MEMS microgripper, force feedback

The International Journal of Robotics Research
Vol. 28, No. 8, August 2009, pp. 1065–1076
DOI: 10.1177/0278364909340212

Figures 1, 2, 4, 7, 11, 13–15 appear in color online: http://ijr.sagepub.com

1. Introduction

Manipulation of single living cells represents an enabling technology that is important for a range of biological disciplines such as genetics (Sun and Nelson 2002; Kallio et al. 2007; Wang et al. 2007), *in vitro* fertilization (Kimura and Yanagimachi 1995), cell mechanical characterization (Sun et al. 2003), and single-cell-based sensing (Whelan and Zare 2003). The past decade has witnessed significant progress in the development of robotic systems and tools for conducting complex cell manipulation tasks, such as probing, characterizing, grasping, and injecting single cells.

Robotic cell manipulation is universally conducted under an optical microscope; thus, visual feedback is the main sensing modality in existing microrobotic cell manipulation systems. Meanwhile, owing to the fact that biological cells are delicate and highly deformable, quantification of interaction forces between the end-effector and cells can enhance the capability of a robotic cell manipulation system. For example, cellular force feedback proved useful for the alignment between a probe and a cell (Sun et al. 2003). The measurement of cellular forces was also demonstrated to enable the prediction of membrane penetration in the injection of zebrafish embryos (Huang et al. 2007; Lu et al. 2007; Pillarisetti et al. 2007).

In order to obtain cellular force feedback during microrobotic cell manipulation, the development of force sensing devices has been a focus, resulting in capacitive force sensors (Sun et al. 2003), piezoresistive sensors (Arai et al. 1999), and piezoelectric force sensors (Shen et al. 2004; Kim et al. 2006; Pillarisetti et al. 2007). There are some inherent limitations that prevent their use in practical cell manipulation tasks including the following: (1) these force sensors are typically limited to resolving forces at the micronewton level while the manipulation of most cell types requires a resolution of nanonewton or sub-nanonewton; and (2) the integration of an end-effector (e.g. glass micropipette) and the force sensors is via epoxy glue, complicating the task of end-effector replace-

ment. Atomic force microscopy (AFM) is capable of providing nanonewton–piconewton force feedback for cellular force measurement and cell manipulation (Dimitriadis et al. 2002; Chen et al. 2007); however, AFM-based manipulation does not provide truly simultaneous imaging and manipulation capabilities. Owing to this limitation, end-effectors used in AFM are limited to micro-cantilever beams with a sharp tip that is required for imaging nano-scale features.

In this paper we present two experimental techniques involving microfabricated devices for nanonewton force sensing and control in two microrobotic cell manipulation tasks. Overcoming limitations of existing cellular force sensing approaches, a vision-based cellular force measurement technique with a nanonewton force resolution is reported, employing a microfabricated elastic cell holding device and a sub-pixel visual tracking algorithm. The technique allows for accurately resolving cellular forces during microrobotic cell manipulation without disturbing the manipulation process or imposing difficulties in end-effector replacement. The effectiveness of the technique is demonstrated in microrobotic mouse embryo injection. Furthermore, the force sensing technique proves that the measured mechanical difference could be useful for *in situ* distinguishing of normal embryos from those with compromised developmental competence, without requiring a separate cell characterization process.

Centered upon cellular force sensing and control, this paper also presents force-controlled micrograsping of biological cells at the nanonewton force level. As mechanical end-effectors, microgrippers enable the pick–transport–place of biological cells in an aqueous environment. The microrobotic system employs a novel microgripper that integrates two-axis force sensors for resolving both gripping forces and contact forces between the gripping arm tips and a sample/substrate. The force-controlled microrobotic system experimentally demonstrated the capability of rapid contact detection and reliable force-controlled micrograsping of porcine aortic valve interstitial cells (PAVICs) to accommodate variations in sizes and mechanical properties of cells with a high reproducibility.

This paper was partially presented at the *2008 Robotics: Science and Systems Conference* (Liu et al. 2008). In this journal version, more experimental results and technical details are given. The paper is organized as follows. In Section 2, a vision-based cellular force measurement technique is presented and applied to resolving cellular forces of mouse embryos during microinjection. Nanonewton force-controlled micrograsping of interstitial cells is then described in Section 3. Finally, conclusions are given in Section 4.

2. Vision-based Cellular Force Measurement During Cell Injection

Vision-based force measurement techniques are capable of retrieving both vision and force information from a single vision sensor (charge-coupled device (CCD) or complementary metal–oxide–semiconductor (CMOS) camera) under microscopic environments (Greminger and Nelson 2004; Ammi et al. 2006; Dobrokhotov et al. 2008). For cellular force sensing during microrobotic cell manipulation, this concept is realized by visually tracking flexible structural deformations and, subsequently, transforming material deformations into forces.

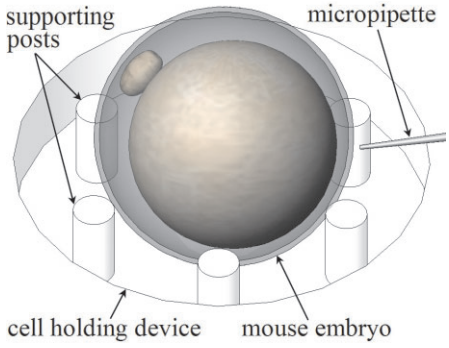

Fig. 1. Cellular force measurement using low-stiffness elastic posts during microrobotic cell injection.

Figure 1 schematically illustrates the principle of vision-based cellular force measurement using an elastic cell holding device during microrobotic cell injection. While the micropipette injects individual cells inside cavities on a cell holding device, applied forces are transmitted to low-stiffness, supporting posts. In real time, a sub-pixel visual tracking algorithm measures post deflections that are fitted into an analytical mechanics model to calculate the force exerted on the cell.

We previously demonstrated this technique on zebrafish embryos (Liu et al. 2007). The study presented in this paper focuses on investigating the feasibility of further miniaturizing the cell holding devices to accommodate mouse embryos (100 μm in diameter versus 1.3 mm zebrafish embryos) for resolving nanonewton cellular forces during microinjection; and the possibility of using cellular force information to distinguish normal mouse embryos from those with compromised developmental competence for better selecting healthy embryos in genetics and reproductive research.

2.1. Microrobotic Mouse Embryo Injection System

The microrobotic mouse embryo injection system (Figure 2) consists of a polydimethylsiloxane (PDMS) cell holding device, an inverted microscope (TE2000, Nikon) with a CMOS camera (A601f, Basler), a three-degree-of-freedom (3-DOF) microrobot (MP-285, Sutter) for controlling the micropipette motion, a motorized X–Y stage (ProScan II, Prior Scientific) for positioning cell samples, and a temperature-controlled chamber (Solent Scientific) to maintain cells at 37°C.

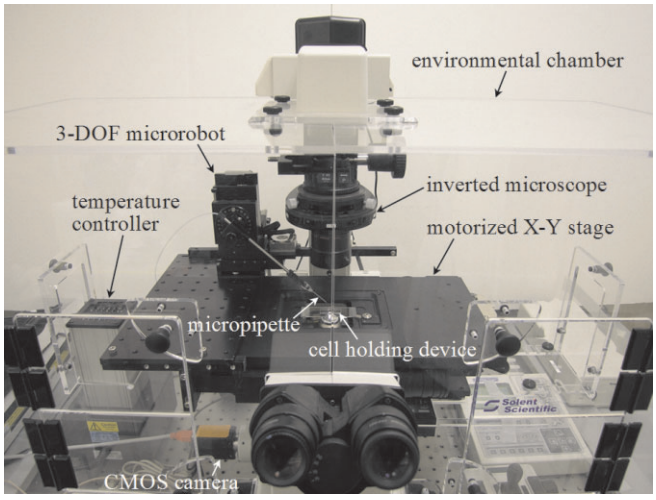

Fig. 2. Microrobotic mouse embryo injection system.

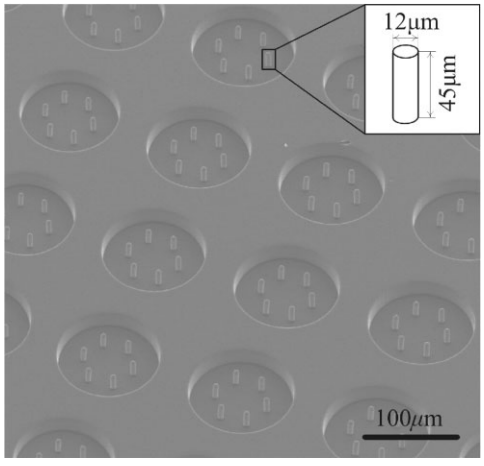

Fig. 3. Scanning electron microscopy (SEM) image of a PDMS cell holding device.

2.2. Fabrication and Characterization of Cell Holding Devices

The cell holding device shown in Figure 3 was constructed with PDMS via soft lithography (Liu et al. 2007). Briefly, PDMS prepolymer prepared by mixing Sylgard 184 (Dow Corning) and its curing agent with a weight ratio of 15:1, was poured over a SU-8 mold (SU-8 50, MicroChem) made on a silicon wafter using standard photolithography. After curing at 80°C for 8 hours, the PDMS devices were peeled off the SU-8 mold. The depth of the cavity and protruding posts is 45 μm, and the diameter of the posts is 12 μm (Figure 3). In order to make the PDMS surface hydrophilic, the devices were oxygen plasma treated for 10 s before use.

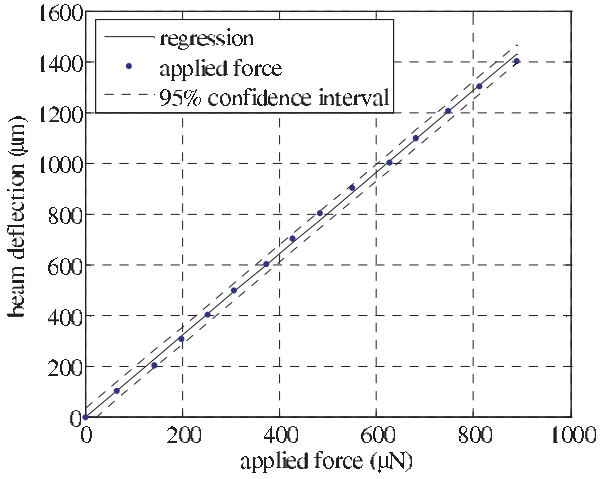

Fig. 4. Young's modulus calibration on a bulkier PDMS beam.

The mechanics model for mapping post deflections into cellular forces, discussed in Section 2.4, requires the Young's modulus of the cell holding device to be accurately calibrated. A bulkier PDMS beam produced under exactly the same microfabrication conditions was calibrated with a piezoresistive force sensor (AE801, SensorOne; sensitivity: 0.909 $\pm$ 0.002 mV mN^{-1}) as described by Liu et al. (2007). It has been demonstrated that the Young's modulus values characterized from bulk PDMS and a micro PDMS structure, both constructed with the same microfabrication parameters, differ within 5% (Zhao et al. 2006). Figure 4 shows the calibration data of applied force versus beam deflection together with least-squares fitting. The determined Young's modulus value is 422.4 kPa.

2.3. Mouse Embryo Preparation

As a model organism, the mouse is a primary animal for genetics and reproductive research. In addition to the importance in *in vitro* fertilization, microinjection of mouse oocytes and embryos is important for screening molecular targets linked to the study of basic biology of embryo development, such as mitochondrial-associated recombinant proteins, neutralizing antibodies, morpholinos, and expression vectors for siRNA.

Normal mouse embryos and defective embryos with blastomere fragmentation were used in the experiments for cellular force measurements. Blastomere fragmentation is often indicative of future programmed cell death (Jurisicova et al. 1996). Although the blastomere fragmented embryo can be distinguished morphologically from normal embryos, using morphological differences alone is not always effective to distinguish between many types of diseased embryos and normal embryos. Thus, the hypothesis to test is whether subtle changes

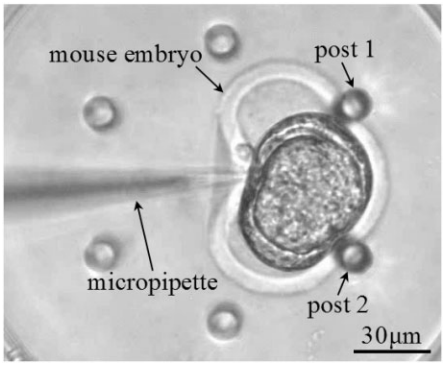

Fig. 5. Indentation forces deform the mouse embryo and deflect two supporting posts.

in the cytoskeleton structure can lead to stiffness changes between abnormal and normal embryos. Thus, cellular force–deformation measurements can possibly provide additional information for detecting embryonic dysfunctions and, therefore, help in better selecting healthy embryos for implantation after microinjection.

The mouse embryos used in this research were collected according to standard protocols approved by the Mount Sinai Hospital Animal Care Committee in Toronto. Young (8–12 weeks old) and older (40 weeks old) imprinting-control-region (ICR) female mice were used for obtaining normal embryos and those with blastomere fragmentation. ICR females with different ages were superovulated by injecting equine pregnant mare's serum gonadotropin (PMSG) and human chorionic gonadotropin (hCG) 48 hours later. The mice were subsequently mated with ICR males of proven fertility, and plugs were verified the next morning. *In vivo* fertilized embryos were collected from the mated female mice at 24 hours post-hCG and cultured in human tubal fluid (HTF) to two-cell stage (at 48 hours post-hCG). The average diameter of the mouse embryos is 98 μm.

2.4. Force Analysis

Figure 5 shows a snapshot captured in the cell injection process. The microrobot controls an injection micropipette to exert an indentation force to a mouse embryo, deflecting the two supporting posts on the opposite side. Post deflections, measured by a visual tracking algorithm that is discussed in Section 2.5, are fitted to an analytical mechanics model to obtain contact forces between the cell and posts. Based on the contact forces, the indentation force applied by the micropipette on the cell is determined through the following force analysis.

The cell is treated as elastic due to the fact that rapid indentation by the micropipette does not leave sufficient time for

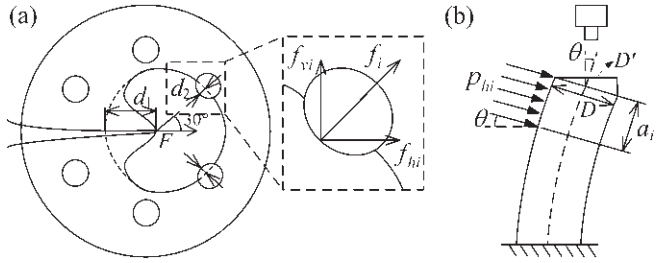

Fig. 6. Injection force analysis. (a) Force balance on the cell under indentation. (b) Post deflection model.

cellular creep or relaxation to occur. Consequently, the injection force, F, is balanced by the horizontal components, f_{hi}, of contact forces between the cell and the two supporting posts (Figure 6(a)),

$$F = \sum_{i=1}^{2} f_{hi}. \tag{1}$$

Much higher deformability of mouse embryos than that of zebrafish embryos results in different contact behavior between a cell and supporting posts, necessitating different treatments of forces in the analysis. In the device configuration, the radius of the cell ($\sim$49 μm) is larger than the depth of the cavity and posts (45 μm), resulting in an initial point contact between the cell and supporting posts before post deflections occur. However, the high deformability of mouse embryos makes the cell membrane conform to the posts when an injection force is applied to the cell. It is assumed that the contact forces are evenly distributed over the contact areas. Thus, the horizontal components, f_{hi}, are expressed by a constant force intensity, p_{hi}, and a contact length, a_i (Figure 6(b)),

$$f_{hi} = p_{hi} a_i. \tag{2}$$

The slope θ of the posts' free ends shown in Figure 6(b) was visually measured to verify the validity of linear elasticity that requires small structural deflections, where $\theta = \cos^{-1}(D'/D)$. The maximum slope was determined to be 11.1°, which satisfies $sin\theta \approx \theta$; thus, the small deflection assumption of linear elasticity holds (Ugural and Fenster 2003). Therefore, the relationship of the horizontal force intensity, p_{hi}, and post deflections can be established (Ugural and Fenster 2003) as

$$p_{hi} = \frac{\delta_i}{40a_i(1+\gamma)(2H-a_i)/9\pi ED^2 + 8(a_i^4 + 8H^3 a_i - 6H^2 a_i^2)/3\pi ED^4}, \tag{3}$$

where $i = 1, 2$, δ_i is the horizontal deflection, H and D are the post height and diameter and E and γ are Young's modulus and Poisson's ratio ($\gamma = 0.5$ for PDMS).

Combining (1)–(3) yields the injection force applied by the micropipette to the cell,

$$F = \sum_{i=1}^{2} \frac{\delta_i a_i}{40a_i(1+\gamma)(2H-a_i)/9\pi ED^2 + 8(a_i^4 + 8H^3 a_i - 6H^2 a_i^2)/3\pi ED^4}. \tag{4}$$

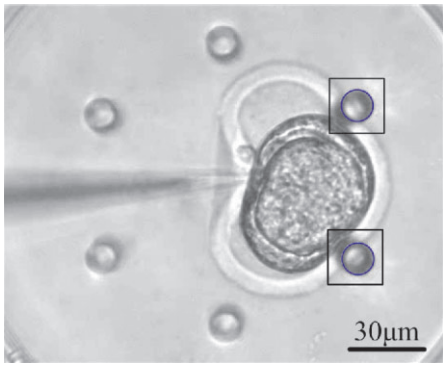

Fig. 7. Image patches tracked by template matching and LSCD detected post top circles.

In (4), the unknown parameters are the post horizontal deflections, δ_i, and the contact length, a_i. Experimentally, imaging with a side-view microscope confirmed that the contact length, a_i, increases at a constant speed, υ, for a given indentation speed. Hence, $a_i = \upsilon t$, where t denotes time.

For a constant indentation speed of the micropipette, υ varies for different cells. At an indentation speed of 20 μm s^{-1} used throughout the experiments, υ values of the 10 tested mouse embryos were measured to be 0.8–1.2 μm s^{-1}. It was found that the sensitivity of the mechanics model (4) to variations in υ is low. The injection force varies only by 1% when υ changes from 0.8 to 1.2 μm s^{-1}. Thus, the average value of the measured speeds, 1 μm s^{-1} was used to calculate injection forces for all of the embryos.

2.5. Visual Tracking of Post Deflections

In order to accurately track post deflections, a visual tracking algorithm with a resolution of 0.5 pixels was developed and described in detail by Liu et al. (2007). A template matching algorithm with constant template updates first tracks the motion of the supporting posts, providing processing areas for a least-squares circle detection (LSCD) algorithm to determine the center positions of the posts. The LSCD algorithm utilizes a Canny edge detector to obtain an edge image and then extracts a portion of the top surface of the post for circle fitting. Figure 7 shows the tracked image patches and LSCD detected post top circles.

2.6. Experimental Results

As mouse embryos are exquisitely sensitive to slight temperature variations, experiments were conducted at 37°C inside the temperature-controlled chamber. With a 40× objective (NA 0.55), the pixel size of the imaging system was calibrated to be 0.36 × 0.36 μ m^2. Micropipette tips used for indenting mouse embryos was 1.8 μm in diameter.

Table 1. Slopes of Cellular Force-Deformation Curves.

mouse embryo	slope (nN/μm)	slope average ± deviation (nN/μm)
normal embryo 1	3.35	
normal embryo 2	2.74	
normal embryo 3	2.52	3.02 ± 0.40
normal embryo 4	3.46	
normal embryo 5	3.03	
fragmented embryo	1.84	
fragmented embryo	1.45	
fragmented embryo	1.81	1.59 ± 0.24
fragmented embryo	1.57	
fragmented embryo	1.26	

Five normal ICR embryos and five ICR embryos with blastomere fragmentation at the two-cell stage, as shown in Figure 8, were used for cellular force measurements. The 10 embryos were manually delivered onto the cell holding device using a transfer pipette and then indented via microrobotic teleoperation. The micropipette was controlled to indent each embryo by 30 μm at 20 μm s^{-1}. During the indentation process, force data were collected in real time (30 data points per second).

Figure 9 shows force–deformation curves of both normal and fragmented embryos. The horizontal axis represents cell deformation, $d = d_1 + d_2 \cos 30^\circ$, where d_1 and d_2 were defined in Figure 6. The vertical axis shows vision-based cellular force data. With the current cell holding devices and imaging system, the force measurement resolution was determined to be 3.7 nN.

From Figure 9, it can be seen that the force–deformation curves of normal and fragmented embryos separate themselves into two distinct regions. Table 1 summarizes the curve slopes calculated by linear regression. The slopes for normal embryos range from 2.52 to 3.46 nN μm^{-1} while the slopes for fragmented embryos are between 1.26 and 1.84 nN μm^{-1}, quantitatively demonstrating that the normal embryos and fragmented embryos are mechanically different.

All of the indented embryos were subsequently cultured in an incubator at 37°C with 5% CO_2. The five normal embryos successfully developed into the four-cell stage; however, all of the five fragmented embryos were arrested at the two-cell stage, proving that the cellular force measurement results may be useful for distinguishing normal embryos from those with embryonic defects during microrobotic cell injection without a separate cell characterization process. Our current study in-

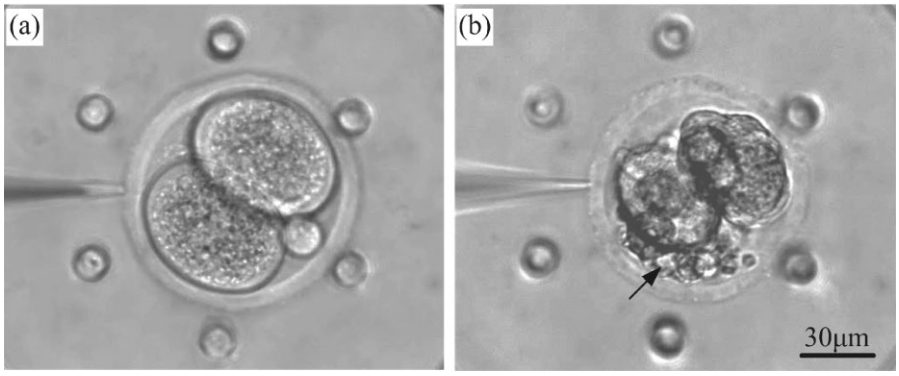

Fig. 8. Mouse embryos for cellular force measurement. (a) Normal embryo. (b) Embryo with blastomere fragmentation (indicated by an arrow).

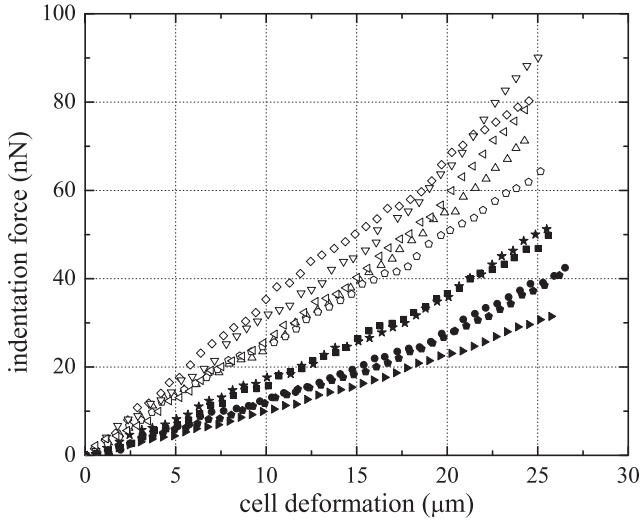

Fig. 9. Force–deformation curves of normal embryos (hollow symbols) and fragmented embryos (solid symbols). They separate themselves into two distinct regions.

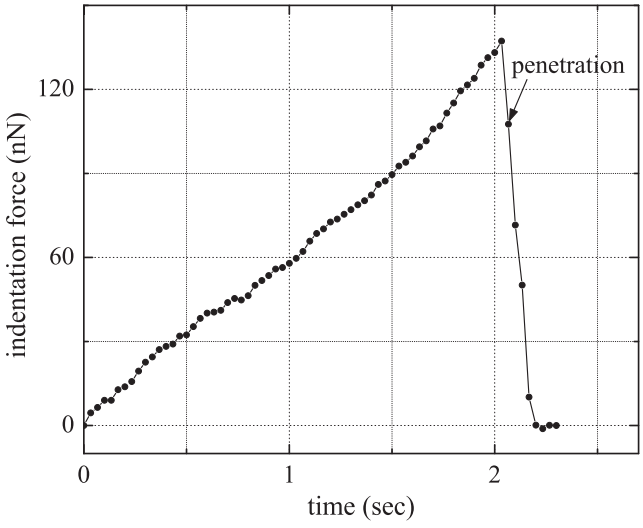

Fig. 10. Cellular force curve of a normal mouse embryo during microrobotic injection. The abrupt force change indicates cell membrane penetration.

volves force quantification on a larger sample size, followed by biological assays to understand underlying mechanisms of embryo mechanical changes.

In addition, the cellular force sensing technique can also be used for detecting the penetration of cell membrane in microrobotic cell injection. An abrupt change of cellular forces (Figure 10) indicates cell membrane penetration for subsequent material deposition. The average force required to penetrate the outside membrane (*zona pellucida*) of a healthy ICR mouse embryo was determined to be 137.3 nN.

3. Nanonewton Force-controlled Micrograsping of Biological Cells

Compared with end-effectors with a single tip such as a probe or a micropipette for microrobotic cell manipulation, a microgripper with two gripping arms is a more suitable tool for reliable pick–transport–place tasks. Previously demonstrated pick–transport–place of micro-objects using a single probe (Gorman and Dagalakis 2006) took advantage of adhesion forces. The process is affected by many factors such as sample type and size, temperature, and humidity, resulting in poor reliability/reproducibility. Furthermore, the probe-based approach is not applicable to picking up biological cells since adhe-

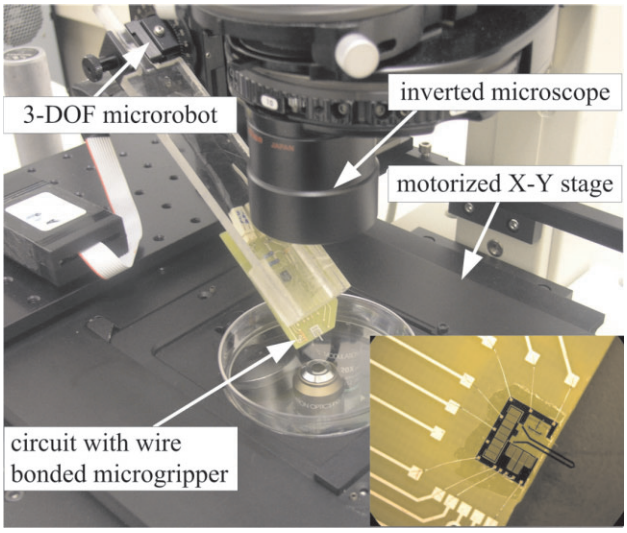

Fig. 11. Microrobotic system for force-controlled micrograsping. The inset picture shows a wire-bonded microgripper.

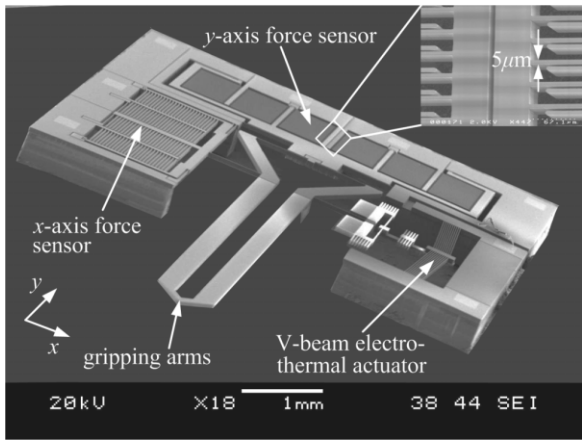

Fig. 12. MEMS-based microgripper with integrated two-axis capacitive force sensors.

sion forces become less significant in an aqueous environment where biological cells survive.

We recently reported the design, microfabrication, and characterization of monolithic microelectromechanical systems (MEMS)-based microgrippers with integrated two-axis force sensors (Kim et al. 2008). In this section we present the application of the force feedback microgrippers to force-controlled micrograsping of biological cells at the nanonewton force level.

3.1. Microrobotic System for Force-controlled Micrograsping

3.1.1. System Setup

The microrobotic system shown in Figure 11 consists of a microgripper wire bonded on a circuit board, a 3-DOF microrobot (MP-285, Sutter) for positioning the microgripper, a motorized X–Y stage (ProScan II, Prior Scientific) for positioning cell samples, an inverted microscope (TE2000, Nikon) with a CMOS camera (A601f, Basler), and a motion control board (6259, National Instruments) mounted on a host computer. The microgripper was tilted at an angle of 40° to enable the gripping arm tips to reach samples on the substrate without immersing the actuator or force sensors into the culture medium.

3.1.2. MEMS Microgrippers

Force-controlled micromanipulation requires microgrippers ideally capable of providing multi-axis force feedback: to protect the fragile microgripper by detecting contact between the microgripper and object to be manipulated; and to provide gripping force feedback for achieving secured grasping without applying excessive forces to the object. Many MEMS microgrippers have been developed; however, most of previous devices (Kim et al. 1992; Chronics and Lee 2005; Carlson et al. 2007) had no force sensing capabilities.

Recently reported monolithic MEMS microgrippers employed an electrostatic actuator and a single-axis capacitive force sensor for manipulating micro-objects (Beyeler et al. 2007 and Femto Tools, Switzerland) and for investigating charge transport of DNA (Yamahata et al. 2008). However, no closed-loop force control was demonstrated. The lack of force sensing capabilities along the normal direction for detecting contact forces also makes the microgrippers more prone to device damage during manipulation.

The MEMS microgripper with integrated two-axis force sensors, shown in Figure 12 was constructed through a modified DRIE-SOI process (Kim et al. 2008). The device employs a V-beam electrothermal actuator that is connected to the lower part of a long gripping arm to generate large gripping displacements at gripping arm tips with low driving voltages. The two gripping arm tips are normally closed with an initial opening of 5 μm. When actuated, the active gripping arm is pulled open. The microgripper is capable of securely grasping objects with sizes of 6–72 μm. Figure 13 shows the calibration results of the gripping arm tip displacement and temperature at actuation voltages of 0–10 V. The tip temperature was measured using a fine-gauge thermocouple (CHCO, Omega) with a junction 33 μm in diameter (Figure 14). Each actuation voltage was applied for 30 min to allow the gripping arm to reach thermal equilibrium. From Figure 13, one can see that the gripping arm tip moves by 32 μm at 6 V; and due to the many heat sink beams, the measured temperature at the gripping arm tip is 29°C in air, demonstrating a low temperature suitable for biomaterial manipulation.

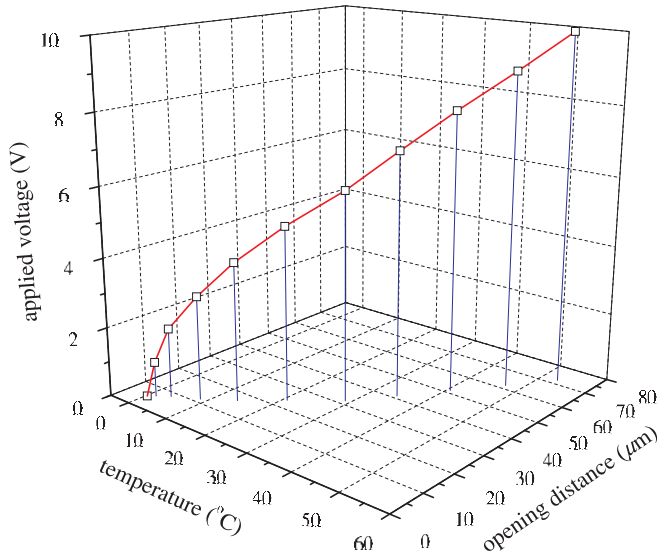

Fig. 13. Measured gripping arm tip displacement and temperature at actuation voltages of 0–10 V.

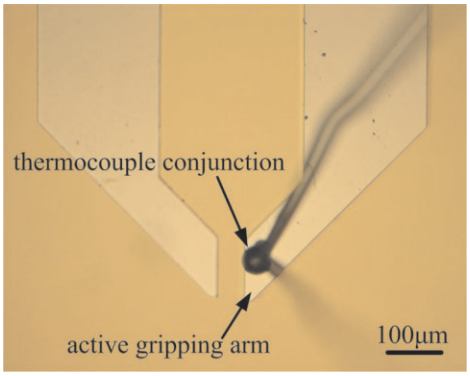

Fig. 14. A snapshot showing the setup for temperature measurement.

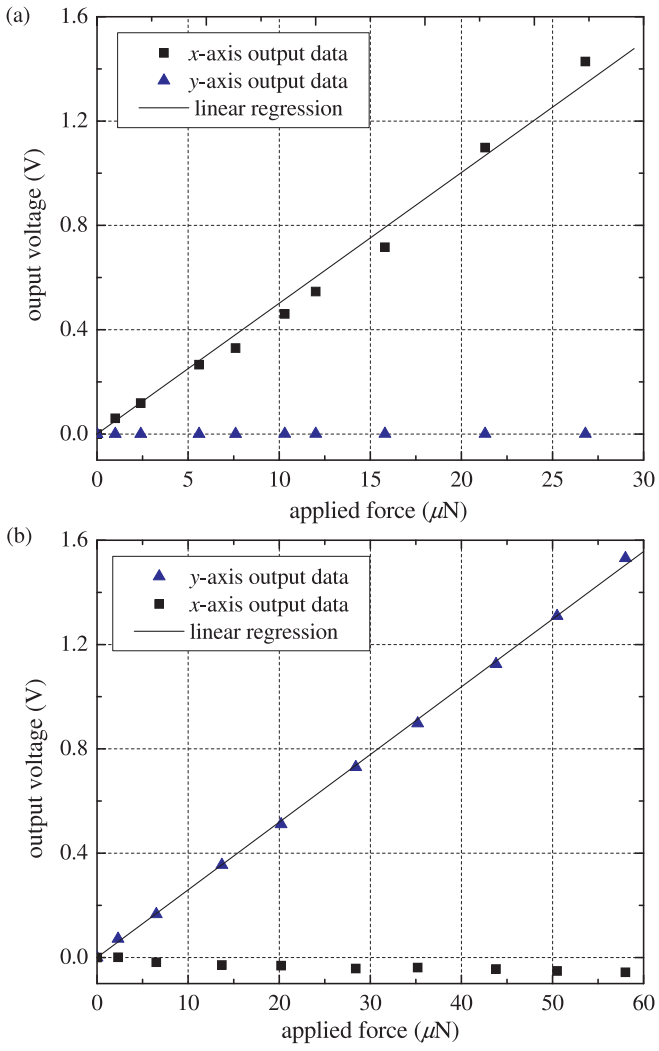

Fig. 15. Force sensor calibration results. Forces applied: (a) only along the x direction; (b) only along the y direction. Also shown are the coupled responses.

Integrated two-axis capacitive force sensors were implemented with transverse differential comb drives (Sun et al. 2005) and were configured orthogonally. The contact force feedback (y-directional) enables contact detection and protects the microgripper from breakage. The gripping force feedback (x-directional) permits force-controlled micrograsping with a force controller to accommodate size and stiffness variations of objects to achieve secured grasping with no excessive forces applied. The force sensors were calibrated using a precision microbalance (XS105DU, Mettler Toledo) with a resolution of 0.1 μN. Figure 15 shows the force sensor calibration results, demonstrating a high input–output linearity and minimized cross-axis coupling. The sensitivity of the two force sensors is 0.05 V N^{-1} (x-axis) and 0.026 V N^{-1} (y-axis). The integrated force sensors are capable of resolving contact forces up to 58 μN (resolution: 38.5 nN at 15Hz) and gripping forces up to 30 μN (resolution 19.9 nN at 15Hz).

3.2. Interstitial Cell Preparation

PAVICs were manipulated to demonstrate force-controlled micrograsping. Manipulation of single PAVICs with cellular force feedback is required for cell transfer and mechanical characterization in pharmacological studies, such as for the understanding and treatment of heart aortic valve calcification.

Aortic valve leaflets were harvested from healthy pig hearts obtained from a local abattoir. After rinsing with antibiotics, each leaflet was treated with collagenase (150 U ml^{-1}, 37°C, 20 min) and the leaflet surfaces were scraped to remove endothelial cells. The leaflets were then minced, and digested with collagenase (150 U ml^{-1}, 37°C, 2 hours). The interstitial cells were enzymatically isolated, grown on tissue culture flasks, and kept in an incubator in standard tissue culture medium (Dulbecco's modified eagle's medium (DMEM) supplemented with 10% fetal bovine serum (FBS) and 1% antibiotics). The medium was changed every 2 days, and the cells were passaged when confluent. Passage 2 cells were trypsinized and re-suspended in standard tissue culture medium at 10^5 cells ml^{-1} for use in experiments.

3.3. Experimental Results

In order to reduce adhesion of cells to the gripping arm tips and, thus, facilitate cell release, the microgripper tips were dip coated with 10% SurfaSil siliconizing fluid (Pierce Chemicals) and 90% histological-grade xylenes (Sigma-Aldrich) for 10 s before use.

3.3.1. Contact Detection

Contact detection is enabled by monitoring the contact force feedback. An alternative possibility for contact detection is to measure impedance between an end-effector and cells/substrate (Kallio et al. 2007). A droplet of cell culture medium containing suspended PAVICs (10–20 μm in diameter) was dispensed through pipetting onto a polystyrene Petri dish. After PAVICs settled down on the substrate, a microrobot controlled the microgripper to immerse gripping arm tips into the liquid droplet and conducts contact detection.

Contact detection is important to protect the microgripper from damage. After the tips of gripping arms were immersed into the medium, the microrobot controlled the microgripper at a constant speed of 20 μm s^{-1} to approach the substrate while force data along the y direction were sampled. The contact detection process completes within 5 s. Without the integrated contact force sensor, this process would be highly time consuming and operator skill dependent.

When the monitored contact force level reaches a pre-set threshold value, it indicates that contact between the gripping arm tips and the substrate is established. Subsequently, the microrobot stops lowering the microgripper further, waits for 1.2 s, and moves the microgripper upwards until the contact force returns to zero (Figure 16). The pre-set threshold force value used in the experiments was 150 nN, which was effective for reliably determining the initial contact between the gripping arm tips and the substrate. After the initial contact position is detected, the microgripper is positioned a few micrometers above the detected contact position for force-controlled micrograsping. The 50 μm thick gripping arms guaranteed secured grasping of PAVICs with different sizes.

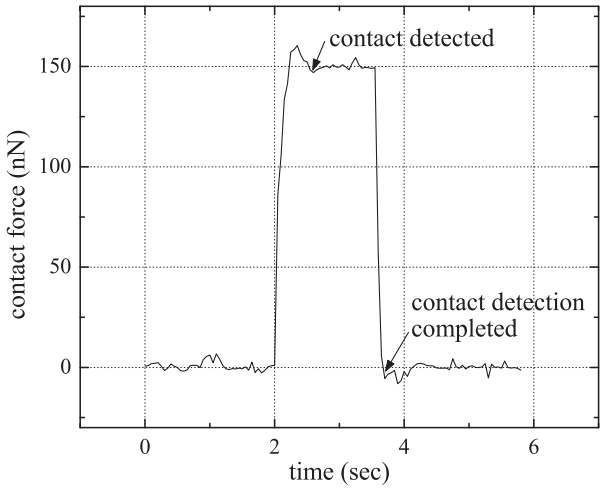

Fig. 16. Contact force monitoring for reliable contact detection.

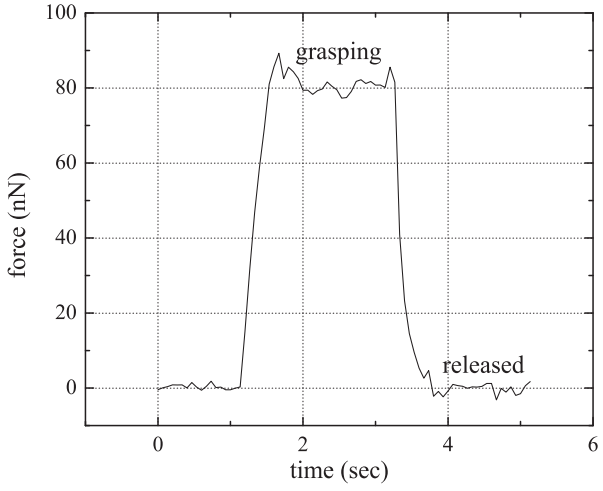

Fig. 17. Gripping force profile during micrograsping and releasing of a cell.

3.3.2. Force-controlled Cell Grasping

Before the system performed force-controlled micrograsping of PAVICs, experiments were conducted to evaluate the effectiveness of open-loop micrograsping. The system applies a voltage to the V-beam electrothermal actuator to produce an opening larger than the size of a PAVIC between the two gripping arms. When grasping a target PAVIC, the system reduces the applied voltage level, which decreases the arm opening for grasping.

Figure 17 shows the force profile during cell grasping and releasing, where a sequence of actuation voltages was applied (5 V opening voltage, 1.5 V grasping voltage, and 5 V releasing voltage) to grasp and release a 14 μm PAVIC. At 1.5 V

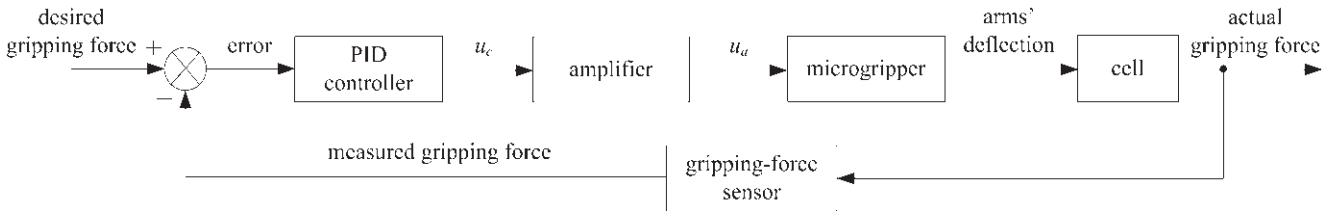

Fig. 18. Block diagram of force-controlled micrograsping.

grasping voltage, the PAVIC was experiencing a gripping force of 80 nN that produced 12% cell deformation of its diameter. Owing to different sizes of PAVICs and their stiffness variations, a single fixed grasping voltage often caused either unsecured grasping or cell rupturing from excessively applied forces, necessitating closed-loop force-controlled micrograsping.

A closed-loop control system was implemented by using gripping force signals as feedback. Figure 18 shows the block diagram of the force control system that accepts a pre-set force level as reference input and employs proportional–integral–derivative (PID) control for force-controlled micrograsping. Figure 19(a) shows the step response of the force-controlled micrograsping system to track a reference input of 80 nN. The settling time is approximately 200 ms. Corresponding to reference input force steps with an increment of 40 nN, tracking results are shown in Figure 19(b).

Enabled by the monolithic microgripper with two-axis force feedback, the microrobotic system demonstrates the capability of rapidly detecting contact, accurately tracking nanonewton gripping forces, and performing reliable force-controlled micrograsping to accommodate size and mechanical property variations of objects. Figure 20 shows three PAVICs of different sizes that were picked, placed, and aligned. Force-controlled micrograsping of the aligned PAVICs was conducted at a force level of 65 nN.

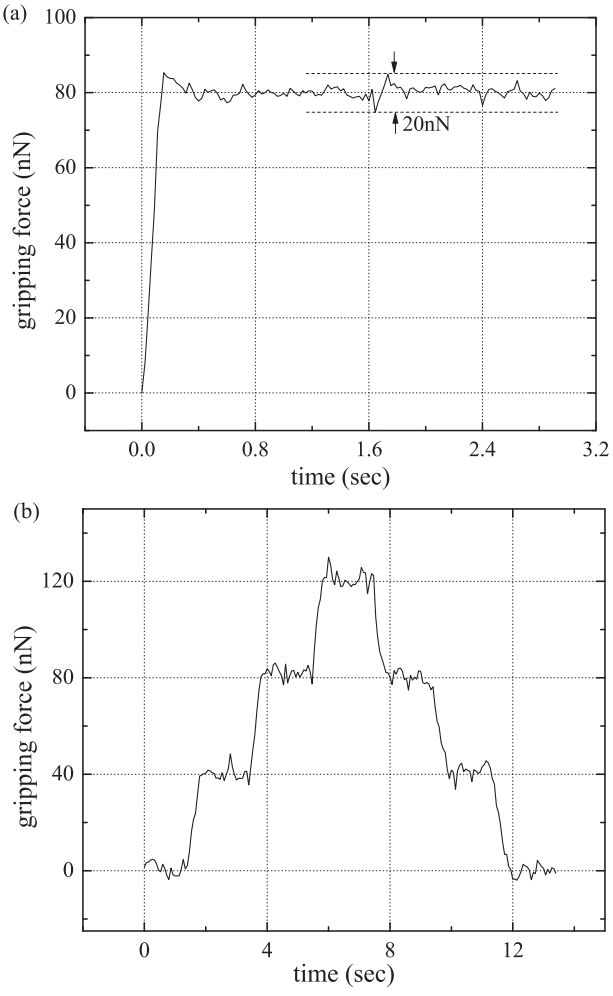

Fig. 19. (a) Step response of force-controlled micrograsping. (b) Tracking force steps with an increment of 40 nN.

4. Conclusion

Using two embodiments of microrobotic cell manipulation (i.e. microinjection and pick–transport–place), in this paper we have reported two techniques involving microfabricated devices for accurately sensing and controlling the interaction forces in microrobotic cell manipulation at the nanonewton level.

Based on polymeric cell holding microdevices, which can be readily integrated into a microrobotic cell manipulation system as force sensors, *in situ* measurement of cellular forces during microinjection has been realized with a nanonewton resolution (3.7 nN). The injection forces have been extracted in real time from visual feedback by tracking the material deformation using a sub-pixel visual tracking algorithm. The cellular force feedback has been demonstrated experimentally to provide two-fold functions in microrobotic cell injection: (1) it can be used to predict the penetration of the cell membrane and, therefore, as a triggering signal for material deposition after penetration; and (2) force–deformation data might prove useful for distinguishing healthy embryos from

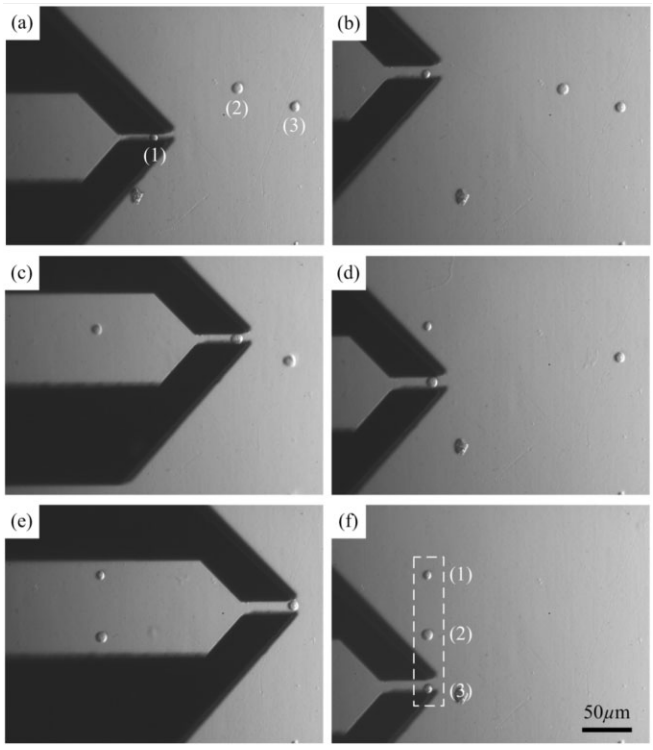

Fig. 20. Cell manipulation and alignment with force-controlled micrograsping. (a) After contact detection, the microgripper grasps a first cell. (b) The microgripper transfers the cell to a new position and releases the cell. (c) The microgripper grasps a second cell. (d) Transferring and releasing the second cell. (e) The microgripper approaches a third cell. (f) Transferring and releasing the third cell. Three cells of different sizes are transferred to desired positions and aligned.

those with compromised development competence during microinjection, without requiring a separate cell characterization process.

Utilizing a force feedback MEMS microgripper, we have also presented nanonewton force-controlled micrograsping of biological cells at a force level of 20 nN at 15Hz. In the force-controlled pick–transport–place process, force feedback again provided two-fold functions: (1) contact force feedback enables rapid, reliable detection of the contact between the substrate and the microgripper arm tips; and (2) gripping force feedback enables accurate closed-loop control of gripping forces to guarantee secured grasping of a cell, yet avoid the application of excessive gripping forces.

Acknowledgments

The authors thank Roxanne Fernandes for the assistance with mouse embryo preparation, and Christopher Moraes for assistance with interstitial cell preparation. This work was supported by the Natural Sciences and Engineering Research Council of Canada, Ontario Centers of Excellence, the Ontario Ministry of Research and Innovation, and the Canada Research Chairs Program.

References

Ammi, M., Ladjal, H. and Ferreira, A. (2006). Evaluation of 3-D pseudo-haptic rendering using vision for cell micromanipulation. *Proceedings IEEE/RSJ International Conference on Intelligent Robots and Systems*, Beijing, China, pp. 2115–2120.

Arai, F., Sugiyama, T., Fukuda, T., Iwata, H. and Itoigawa, K. (1999). Micro tri-axial force sensor for 3D biomicromanipulation. *Proceedings of the IEEE International Conference on Robotics and Automation*, Detroit, MI, pp. 2744–2749.

Beyeler, F., Neild, A., Oberti, S., Bell, D. J., Sun, Y., Dual, J. and Nelson, B. J. (2007). Monolithically fabricated microgripper with integrated force sensor for manipulating microobjects and biological cells aligned in an ultrasonic field. *IEEE/ASME Journal of Microelectromechanical Systems*, **16**(1): 7–15.

Carlson, K., Andersen, K. N., Eichhorn, V., Petersen, D. H., Mølhave, K., Bu, I. Y. Y., Teo, K. B. K., Milne, W. I., Fatikow, S. and Bøggild, P. (2007). A carbon nanofibre scanning probe assembled using an electrothermal microgripper. *Nanotechnology*, **18**: 375501.

Chen, X., Kis, A., Zettl, A. and Bertozzi, C. R. (2007). A cell nanoinjector based on carbon nanotubes. *Proceedings of the National Academy of Sciences of the USA*, **104**(20): 8218–8222. http://www.pnas.org/content/104/20/8218.abstract.

Chronics, N. and Lee, L. P. (2005). Electrothermally activated SU-8 microgripper for single cell manipulation in solution. *IEEE/ASME Journal of Microelectromechanical Systems*, **14**(4): 857–863.

Dimitriadis, E., Horkay, F., Maresca, J., Kachar, B. and Chadwick, R. (2002). Determination of elastic moduli of thin layers of soft material using the atomic force microscope. *Biophysical Journal*, **82**(5): 2798–2810.

Dobrokhotov, V. V., Yazdanpanah, M. M., Pabba, S., Safir, A. and Cohn, R. W. (2008). Visual force sensing with flexible nanowire buckling springs. *Nanotechnology*, **19**(3): 035502.

Gorman, J. J. and Dagalakis, N. G. (2006). Probe-based microscale manipulation and assembly using force feedback. *Proceedings of the 1st Joint Emergency Preparedness and Response/Robotic and Remote Systems Topical Meeting*, Salt Lake City, UT, pp. 621–628.

Greminger, M. A. and Nelson, B. J. (2004). Vision-based force measurement. *IEEE Transactions on Pattern Analysis and Machine Intelligence* 26(3): 290–298.

Huang, H. B., Sun, D., Mills, J. K., and Li, W. J. (2007). Visual-based impedance force control of three-dimensional cell injection system. In *Proceedings of IEEE International Conferernce on Robotics and Automation*, volume 3519. Rome, Italy.

Jurisicova, A., Varmuza, S. and Casper, R. F. (1996). Programmed cell death and human embryo fragmentation. *Molecular Human Reproduction*, **2**(2): 93–98.

Kallio, P., Ritala, T., Lukkari, M. and Kuikka, S. (2007). Injection guidance system for cellular microinjections. *The International Journal of Robotics Research*, **26**(11–12): 1303–1313.

Kim, C. J., Pisano, A. P. and Muller, R. (1992). Silicon-processed overhanging microgripper. *Journal of Microelectromechnical Systems*, **1**(1): 31–36.

Kim, D., Hwang, C., Sun, Y., Lee, S. H., Kim, B. K. and Nelson, B. J. (2006). Mechanical analysis of chorion softening in prehatching stages of zebrafish embryos. *IEEE Transactions on NanoBioScience*, **5**(2): 89–94.

Kim, K. Y., Liu, X. Y., Zhang, Y. and Sun, Y. (2008). Nanonewton force-controlled manipulation of biological cells using a monolithic MEMS microgripper with two-axis force feedback. *Journal of Micromechanics and Microengineering*, **18**(5): 055013.

Kimura, Y. and Yanagimachi, R. (1995). Intracytoplasmic sperm injection in the mouse. *Biology of Reproduction*, **52**(9): 709–720.

Liu, X. Y., Kim, K. Y., Zhang, Y. and Sun, Y. (2008). Nanonewton force sensing and control in microrobotic cell manipulation. *Proceedings of Robotics: Science and Systems Conference*, Zurich, Switzerland.

Liu, X. Y., Sun, Y., Wang, W. H. and Lansdorp, B. M. (2007). Vision-based cellular force measurement using an elastic microfabricated device. *Journal Micromechanics and Microengineering*, **17**(7): 1281–1288.

Lu, Z., Chen, P., Nam, J., Ge, R. and Lin, W. (2007). A micromanipulation system with dynamic force-feedback for automatic batch microinjection. *Journal of Micromechanics Microengineering*, **17**(2): 314–321.

Pillarisetti, A., Pekarev, M., Brooks, A. D.,and Desai, J. P. (2007). Evaluating the effect of force feedback in cell injection. *IEEE Transactions on Automation Science and Engineering*, **4**(3): 322–331.

Shen, Y. T., Xi, N., Lai, K. W. C. and Li, W. J. (2004). A novel PVDF microforce/force rate sensor for practical applications in micromanipulation. *Sensor Review*, **24**(3): 274–283.

Sun, Y., Fry, S. N., Potassek, D. P., Bell, D. J. and Nelson, B. (2005). Characterizing fruit fly flight behavior using a microforce sensor with a new comb drive configuration. *IEEE/ASME Journal of Microelectromechnical Systems*, **14**: 4–11.

Sun, Y. and Nelson, B. J. (2002). Biological cell injection using an autonomous microrobotic system. *The International Journal of Robotics Research*, **21**(10–11): 861–868.

Sun, Y., Wan, K., Nelson, B., Bischof, J. and Roberts, K. (2003). Mechanical property characterization of the mouse zona pellucida. *IEEE Transactions on NanoBioScience*, **2**(4): 279–286.

Ugural, A. C. and Fenster, S. K. (2003). *Advanced Strength and Applied Elasticity*. Englewood Cliffs, NJ, Prentice-Hall.

Wang, W. H., Liu, X. Y., Gelinas, D., Ciruna, B. and Sun, Y. (2007). A fully automated robotic system for microinjection of zebrafish embryos. *PLos ONE*, **2**(9): e862; doi: 10.1371/journal.pone.0000862.

Whelan, R. J. and Zare, R. N. (2003). Single-cell immunosensors for protein detection. *Biosensors and Bioelectronics*, **19**(4): 331–336.

Yamahata, C., Collard, D., Takekawa, T., Kumemura, M., Hashiguchi, G. and Fujita, H. (2008). Humidity dependence of charge transport through DNA revealed by silicon-based nanotweezers manipulation. *Biophysical Journal*, **94**(1): 63–70.

Zhao, Y., Lim, C. C., Sawyer, D. B., Liao, R. and Zhang, X. (2006). Microchip for subcelluar mechanics study in living cells. *Sensors and Actuators B—Chemical*, **114**(2): 1108–1115.